An Amorphous Alloy Magnetic Bus-Based SiC NPC Converter with Inherent Voltage Balancing for Grid Connected Renewable Energy Systems

Shakil Ahamed Khan, *Student Member, IEEE,* Md. Rabiul Islam, *Senior Member, IEEE*, Youguang Guo, *Senior Member, IEEE,* and Jianguo Zhu, *Senior Member, IEEE*

***Abstract*—This paper presents an amorphous alloy magnetic bus-based neutral point clamped (NPC) converter for grid-connected renewable generation systems. In the proposed system, the amorphous alloy high-frequency high-power density multi-winding magnetic bus generates balanced dc supplies for the five-level 5L-NPC converter for high-quality power conversion. Compared to the traditional NPC converter topologies, the proposed magnetic bus-based architecture does not require any control circuit for voltage balancing of the series connected capacitors. The magnetic bus inherently overcomes galvanic isolation issues and may reduce the size of the boosting inductor. In this paper, a finite control set model predictive control (FCS-MPC) algorithm is derived to control the grid-connected 5L-NPC inverter for multilevel voltage synthesizing, while realizing the user-defined active and reactive power values. To verify the proposed concept, a simulation model is developed and analyzed in MATLAB/Simulink environment. To validate the technology a scale down prototype test platform is developed in the laboratory with silicon carbide switching devices which realize high blocking voltage, low power dissipation, high switching frequency and high-temperature operation. Based on the simulation and the experimental results, it is expected that the proposed converter will have a great potential for widespread application in renewable generation systems including superconducting generator-based wind turbines.**

***Index Terms*—Amorphous alloy, magnetic bus, neutral point clamped (NPC) converter, capacitor voltage balancing, control, silicon carbide switching devices, superconducting wind generator.**

I. Introduction

In order to reduce the size and weight of the wind turbine nacelle, the high temperature superconducting (HTS) cable based generator has been gaining significant interest in recent years [1]–[7]. The weight and volume of superconducting generator based wind turbine can be reduced further by eliminating the heavy and bulky step-up transformer from the nacelle [8]. In recent years, multilevel converters (MCs) have received significant interest to fulfill this objective [9], [10].

In renewable energy generation systems, a conventional power conditioning circuit includes two stages: a dc–dc boost converter and a dc–ac inverter [11], [12]. The dc–ac inverter is usually a two-level full-bridge inverter. Compared to the conventional two-level inverters, MCs such as neutral point clamped (NPC) converters present more advantages, including the better quality of output power, and higher voltage-handling capability using lower rated switching devices [13]–[15]. In recent years, the single-phase NPC inverters have gained significant popularity for their many emerging applications, such as energy storage systems (ESSs), active power filters (APFs), vehicle-to-grid (V2G), grid-to-vehicle (G2V), uninterruptible power supplies (UPSs), and renewable energy conversion systems (RECSs). NPC converter topology consists of a single dc-link in parallel with a series of capacitors [16]. It is required to maintain balanced voltages in the series connected capacitors to generate distortion-less output at the ac side of the NPC inverter. Thus, it is essential to control not only the grid-current variables but also the capacitor voltages of the traditional NPC converters [17], [18]. To accomplish these objectives, a complex control strategy is required.

In order to overcome capacitor voltage unbalancing problem, an advanced magnetic material-based high-frequency magnetic bus is proposed in this paper. The novelty of this approach is the application of magnetic bus to generate the balanced dc supplies for NPC converter. Contrary to the conventional system, the magnetic bus-based design does not require any control method for voltage balancing of the series connected capacitors of the NPC converter. Moreover, the magnetic bus provides the required galvanic isolation and reduces the size of the boosting inductor due to its voltage step-up capability.

The focuses of this paper are the design, implementation, and evaluation of a magnetic bus-based NPC converter and associated control system for grid-connected renewable generation systems. In this paper, a finite control set model predictive control (FCS-MPC) is employed as the inner current tracking controller, and the outer control loop generates the active and reactive power references for the inner FCS-MPC based current tracking controller, while

Manuscript received, August 31, 2018, revised September 25, 2018.

S. A. Khan and Y. G. Guo are with the School of Electrical and Data Engineering, University of Technology Sydney, 81 Broadway, Ultimo, NSW 2007, Australia. e-mails: Shakil.A.Khan@student.uts.edu.au, Youguang.Guo-1@uts.edu.au.

M. R. Islam is with the School of Electrical, Computer and Telecommunications Engineering, Faculty of Engineering and Information Sciences, University of Wollongong, NSW 2522, Australia. e-mails: mrislam@uow.edu.au, rabiulbd@hotmail.com.

J. G. Zhu is with the School of Electrical and Information Engineering, The University of Sydney, Sydney, NSW 2006, Australia. e-mail: Jianguo.zhu@sydney.edu.au.

Color versions of one or more of the figures in this paper are available online at http://ieeexplore.ieee.org.

Digital Object Identifier will be inserted here upon acceptance.

achieving the desired active and reactive power references. To validate the proposed technology, a scale down prototype test platform is developed in the laboratory with silicon carbide (SiC) semiconductor devices which realize high blocking voltage, low power dissipation, high switching frequency and high-temperature operation.

The rest of this paper is organized in the following manner. Section II describes the single-phase grid-connected predictive model of the five-level neutral point clamped (5L-NPC) converter. The FCS-MPC based control technique is described in Section III. Section IV described the amorphous alloy based magnetic bus. Section V presents the simulation results of the 5L-NPC converter while connected to the grid. Section VI presents the experimental results with the scale down prototype. Finally, concluding remarks are presented in Section VII.

II. Mathematical Model and Design of Controller

This section focuses on the control of a single-phase grid-connected 5L-NPC converter which is connected to the utility grid. The dc-side is connected to a renewable energy source by means of a cascaded connection of a full-bridge inverter, a magnetic bus, and full-bridge rectifiers. As a study case, a 5L-NPC inverter topology is considered in this paper. However, five-level full-bridge neutral point clamped inverter (5L-FBNPC), and five-level active neutral point clamped (5L-ANPC) can also be considered. The circuit structure of the employed 5L-NPC converter topology is shown in Fig. 1 [13]. Based on the internal structure of the converter topology, the circuit should be controlled to generate five voltage levels in the grid-side terminals to realize the requirements for low total harmonic distortion (THD) with reduced *dv/dt* stress in the semiconductor devices.

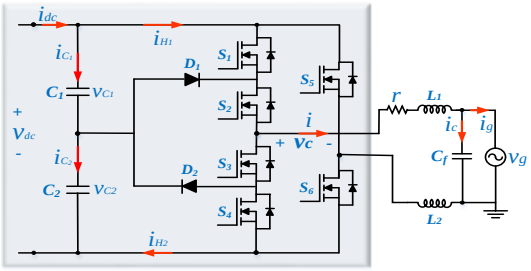

Fig. 1. Topology of the 5L-NPC inverter.

In the proposed power conditioning system, a magnetic bus consisting of winding one as the primary and windings two and three as the secondary are used to generate two isolated and balanced dc supplies by means of two full-bridge rectifiers. These two balanced dc supplies are connected in series in cumulative form to connect the 5L-NPC converter. The mathematical model of the 5L-NPC converter for the dc–ac power conversion stage is presented in the following subsection.

A. Predictive Model of the 5L-NPC Converter

Based on the circuit configuration, the converter should be controlled to generate five voltage levels at the ac-side. The following assumptions are made: a) neglecting conduction losses and switching losses, b) capacitances $C_1$and C_2 have equal values $(C_1 = C_2 = 2C)$, and $L_1 = L_2, (L = L_1 + L_2)$. The continuous-time dynamic model of the employed converter can be expressed via the following equations:

$$v_c(t) = v_{L_1} + v_{L_2} + v_r + v_g = v_L + v_r + v_g \quad (1)$$

$$i = i_c + i_g \quad (2)$$

where $v_c(t) = \psi(t)v_{dc}$, v_g is the grid voltage, v_L is the voltage across the filter inductors, v_r is the voltage across the equivalent series resistance of the filter inductors, v_c represents the converter voltage, i_g denotes the grid current, i_c denotes the grid-side capacitor current, and ψ is the control input which takes the values in the finite set from Table I. Substituting (2) into (1) yields:

$$v_c(t) = L\frac{di}{dt} + ri + v_g = L\frac{di_g}{dt} + LC_f\frac{d^2v_g}{dt^2} + v_g + r(i_g + C_f\frac{dv_g}{dt}) \quad (3)$$

where L denotes the grid side filter inductance, and r denotes the equivalent series resistance of the grid-side inductor L. By using the Euler method with a sampling period T_S, (3) can be expressed as:

$$v_c^{\,k} = \frac{L}{T_S}\left(i_g^{\,k+1} - i_g^{\,k}\right) + \frac{LC_f}{T_S^2}\left(v_g^{\,k+1} - 2v_g^{\,k} + v_g^{\,k-1}\right) + ri_g^{\,k} + \frac{rC_f}{T_S}\left(v_g^{\,k+1} - v_g^{\,k}\right) + v_g^{\,k} \quad (4)$$

where k is discretized t.

TABLE I
POSSIBLE STATES OF THE 5L-NPC CONVERTER

	S_1	S_2	S_3	S_4	S_5	S_6	ψ	v_c
$v_g \geq 0$	0	1	0	0	0	1	1	$+v_{DC}$
	1	1	0	0	0	1	2	$+2v_{DC}$
	0	0	1	1	0	0	1	*0*
$v_g < 0$	0	0	1	0	1	0	-1	$-v_{DC}$
	0	0	1	1	1	0	-1/2	$-2v_{DC}$
	1	1	0	0	1	0	0	*0*

By using mathematical simplifications, (4) can be rewritten in terms of the predicted grid current, $i_g^{\,k+1}$ as:

$$i_g^{\,k+1} = \left(1 - \frac{rT_S}{L}\right)i_g^{\,k} - \left(\frac{C_f}{T_S} + \frac{rC_f}{L}\right)v_g^{\,k+1} + \frac{T_S}{L_f}v_c^{\,k} + \left(\frac{2C_f}{T_S} + \frac{rC_f}{L} - \frac{T_S}{L}\right)v_g^{\,k} - \frac{C_f}{T_S}v_g^{\,k-1} \quad (5)$$

where $v_g^{\,k+1}$ can be obtained as [19]:

$$v_g^{\,k+1} = 3v_g^{\,k} - 3v_g^{\,k-1} + v_g^{\,k-2} \quad (6)$$

The 5L-NPC converter topology consists of a single dc-link in parallel with the series connected capacitors. In a conventional NPC converter (without magnetic bus), an

additional control technique is required to balance the capacitor voltages. The dynamic equations for the series connected capacitor voltages can be expressed as follows:

$$C_1 \frac{dv_{C_1}}{dt} = i_{C_1} = i_{dc} - i_{H_1} \tag{7}$$

$$C_2 \frac{dv_{C_2}}{dt} = i_{C_2} = i_{dc} - i_{H_2} \tag{8}$$

where i_{C_1} and i_{C_2} denote the currents through the capacitors $C_1$and C_2 respectively, i_{H_1} and i_{H_2} denote the internal currents of the inverter, and i_{dc} presents the dc-bus current. Based on the model predictive control requirements, the existing values of i_g, v_g, v_{C_1}, and $v_{C_2}$are essential to predict the future behavior of the grid current i_g. The predictive values of the capacitor voltages of the inverter can be expressed as follows:

$$v_{C_1}{}^{k+1} = v_{C_1}{}^{k} + \frac{T_S}{C_1} i_{H_1}{}^{k} - \frac{T_S}{C_1} i_{dc}{}^{k} \tag{9}$$

$$v_{C_2}{}^{k+1} = v_{C_2}{}^{k} + \frac{T_S}{C_2} i_{H_2}{}^{k} - \frac{T_S}{C_2} i_{dc}{}^{k} \tag{10}$$

Thus, to predict the future behaviour of the grid-current, (5) will be used by the proposed controller. Moreover, in a conventional NPC converter, the predicted values of the capacitor voltages are usually calculated by using (9) and (10).

B. d-q Mathematical Model

The grid voltage v_g, the inductor current i, and the inverter voltage v_c are defined as follows:

$$v_g = v_d \sin(\omega t) + v_q \cos(\omega t) \tag{11}$$

$$i = i_d \sin(\omega t) + i_q \cos(\omega t) \tag{12}$$

$$v_c = v_{cd} \sin(\omega t) + v_{cq} \cos(\omega t) \tag{13}$$

where v_d, i_d and v_{cd} are the d-axis components, and v_q, i_q and v_{cq} are the q-axis components of the grid voltage v_g, the inductor current i, and the inverter voltage vectors v_c, respectively.

The inductor current i and grid voltage v_g can be decomposed in their d and q parts at the grid frequency. Thus, system (1) will become:

$$L \frac{di_d}{dt} = v_{cd} - i_d r + i_q \omega L - v_d \tag{14}$$

$$L \frac{di_q}{dt} = v_{cq} - i_q r - i_d \omega L - v_q \tag{15}$$

In a single-phase system, a virtual two-phase system is usually generated to calculate the instantaneous active and reactive power. The second-order generalized integrator (SOGI) is a widely employed method to generate the orthogonal signal of the single-phase voltage and current signals. The transfer functions of SOGI in s-domain are given as follows:

$$x_\alpha(s) = \frac{k\omega s}{s^2 + k\omega s + \omega^2} x(s) \tag{16}$$

$$x_\beta(s) = \frac{k\omega^2}{s^2 + k\omega s + \omega^2} x(s) \tag{17}$$

where k represents the damping factor.

The performance of SOGI is related to the tunning of parameter k. Applying (16) and (17) to the grid voltage v_g and the current i_g, the orthogonal component of the voltage v_g and current i_g can be presented as follows:

$$v_{g-\alpha} = V_g \sin(\omega t) \tag{18}$$

$$v_{g-\beta} = V_g \sin\left(\omega t + \frac{\pi}{2}\right) \tag{19}$$

$$i_{g-\alpha} = I_g \sin(\omega t + \phi) \tag{20}$$

$$i_{g-\beta} = I_g \sin\left(\omega t + \phi + \frac{\pi}{2}\right) \tag{21}$$

According to the instantaneous power theory, the active power $p^k$and the reactive power $q^k$of single-phase system are defined as:

$$\begin{bmatrix} p^k \\ q^k \end{bmatrix} = \frac{1}{2} \begin{bmatrix} v_{g-d}{}^{k} & v_{g-q}{}^{k} \\ v_{g-q}{}^{k} & -v_{g-d}{}^{k} \end{bmatrix} \begin{bmatrix} i_{g-d}{}^{k} \\ i_{g-q}{}^{k} \end{bmatrix} \tag{22}$$

where v_{g-d}, v_{g-q}, i_{g-d}, and i_{g-q} are the d-axis and q-axis components of the grid voltage and the line current in the dq rotating frame, respectively.

The grid voltage is oriented to d-axis in synchronous reference frame. Thus, the grid-side instantaneous active power p^k and reactive power q^k are given by [20]:

$$p^k = \frac{1}{2} v_{g-d}{}^{k} i_{g-d}{}^{k} \tag{23}$$

$$q^k = -\frac{1}{2} v_{g-d}{}^{k} i_{g-q}{}^{k} \tag{24}$$

To calculate the reference grid current, the quantities in rotating reference frame in (23) and (24) are used. Therefore, the expression for reference grid current is given by:

$$i_g{}^{k} = i_{g-q}{}^{k} \cos(\theta) + i_{g-d}{}^{k} \sin(\theta) \tag{25}$$

The quantities $sin(\theta)$ and $cos(\theta)$ in (25) can be obtained by using phase locked-loop (PLL). In this paper, a dc offset rejection capability based PLL [21] is used to calculate the grid voltage information. Fig. 2 shows the block diagram of the dc-offset rejection based SOGI-PLL.

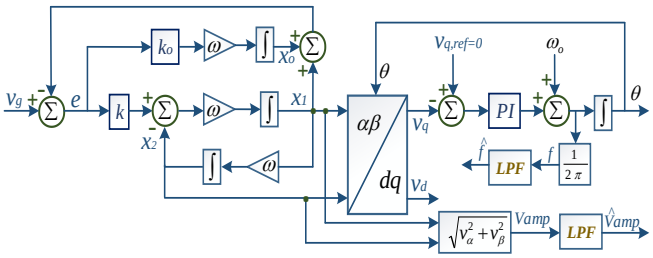

Fig. 2. The dc-offset rejection based SOGI-PLL.

Finally, using (23) and (24), the grid-current references can be expressed as [22]:

$$i_g^{\,k} = \frac{2p^k}{v_{g-d}^{\,k}}\sin(\theta) - \frac{2q^k}{v_{g-d}^{\,k}}\cos(\theta) \tag{26}$$

III. Proposed FCS-MPC for 5L-NPC Converter

This section presents the demonstration of the proposed control system of the magnetic bus-based 5L-NPC converter. The proposed high-frequency magnetic bus-based power conversion systems and the block diagram of the proposed controller are illustrated in Fig. 3.

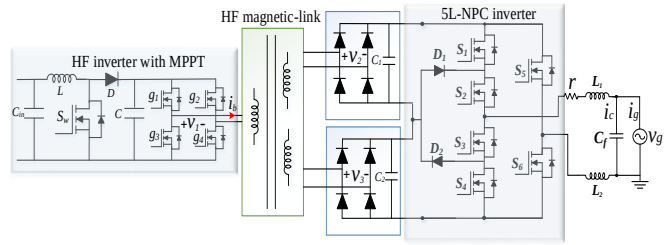

(a)

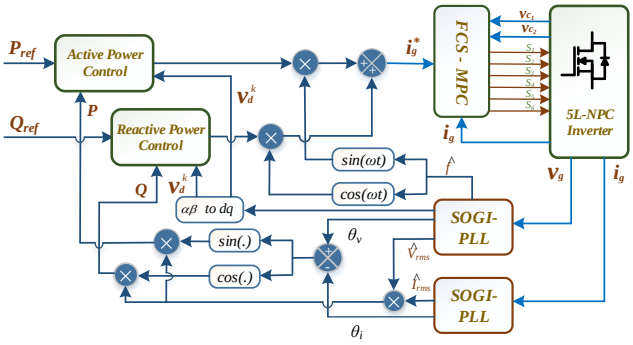

(b)

Fig. 3. (a) Proposed high-frequency magnetic bus-based power conversion system, and (b) block diagram of the 5L-NPC converter control system.

The control objectives regarding the magnetic bus-based single-phase 5L-NPC grid-connected converter are to achieve the desired active and reactive power while generating five distinct voltage level in the ac-side. In the proposed control system, the *d*-axis component (i_d^*) of the current *i* is computed dynamically to maintain the desired active power reference. Similarly, the instantaneous reactive power is calculated by the *q*-axis component (i_q^*) of the current *i*. Therefore, the inverter currents (*d*-axis component (i_d) and *q*-axis component (i_q)) must follow the dynamically calculated references i_d^* and i_q^* to achieve the required control objectives. For the adopted multilevel inverter, the model predictive control with FCS-MPC is used to define the state of the converter in each sampling period. The FCS-MPC offers several advantages, including the possibility to realize multiple control objectives, handling system constraints and the option to include nonlinearities.

A. FCS-MPC for the 5L-NPC Converter

The FCS-MPC algorithm has been derived for current control in the 5L-NPC grid-connected converter drives. The aim of the control system is to track the dynamically calculated grid current reference (i_g^*), while realizing the desired active and reactive power references. The reference grid current i_g^* is calculated from the desired active power reference (P_{ref}) obtained from active power controller and the required reactive power (Q_{ref}) values. To realize these objectives, the FCS-MPC scheme operates in discrete time and uses the discrete model of the adopted inverter topology. The measured system states are used for the state predictions of the control variables for the adopted multilevel inverter model. The state predictions are then evaluated for each of the possible switching states to provide the best performance. It is based on an optimization criterion and uses a cost function which is explained in the following section. Among these switching states, the one which minimizes the cost function is applied to drive the inverter.

B. Cost Function Formulation

In a conventional NPC converter based renewable energy conversion system, it is required to maintain balanced voltage across the series connected capacitors of the NPC inverter for multilevel voltage synthesizing. Therefore, the predicted capacitor voltages are also included in the cost function formulation. The predicted values of the current reference and capacitor voltages at the instant (*k+1*) are calculated at each sampling instant by using (5), (9), and (10) for each of the possible switching states. The cost function is usually defined to control the NPC inverter is given as follows:

$$g_{conv.} = k_i\left(i_g^{*\,k+1} - i_g^{\,k+1}\right)^2 + k_v\left(v_{C_1}^{\,k+1} - v_{C_2}^{\,k+1}\right)^2 \tag{27}$$

The trade-off between the capacitor voltage balancing and the grid-current waveform quality can be achieved by adjusting the weighting factors k_i and k_v in (27). A large value of k_v will take sides in the capacitor voltage balancing by paying the penalty of low THD of the line current, i.e., the quality of the line current highly depends on the voltage balancing of the series capacitors. Furthermore, the weighting factor must be modified dynamically for different operating point of the inverter, which increases the control complexity. Moreover, two additional current sensors are also required to sense the internal currents i_{H_1} and i_{H_2} of the inverter, which increases the design cost. Contrary to the conventional energy conversion system, the proposed magnetic bus-based power converter inherently overcomes the capacitor voltage balancing issues. Only the grid-current variable can be taken into account in the cost function formulation to generate multilevel voltage output for the NPC inverter. The proposed cost function for the adopted 5L-NPC inverter is given as follows:

$$g_{conv.} = \left|i_g^{*\,k+1} - i_g^{\,k+1}\right| \tag{28}$$

Thus, the weighting factor selection and tuning process are not necessary for different operating conditions.

IV. Amorphous Alloy Magnetic-Bus

Amorphous and nanocrystalline materials are advanced soft

magnetic materials and suitable for the development of high-power density core of the high-frequency transformers or magnetic bus due to their excellent electromagnetic properties such as high saturation induction, permeability and electrical resistivity, and low specific core loss and coercive force compared with traditional magnetic materials, e.g. ferrite, silicon steel and permalloy. Amorphous ribbons with a thickness between 15 to 35 µm and a width between 2.5 to 213 mm are produced from molten metal alloy through a rapid solidification process at a cooling rate of approximately one million ºC/s. Metglas, Conway, SC, USA is a world leading producer of amorphous ribbon and is a subsidiary of Hitachi Metals America, Ltd. High-frequency transformer or magnetic bus usually operates under non-sinusoidal, say, square-wave excitations. Metglas commercially develops amorphous ribbon 2605SA1 with saturation induction of 1.56 T and specific core loss of 70 W/kg at 10 kHz square-wave excitation of 0.5 T. Fig. 4 shows the core loss of amorphous alloy 2605SA1 under square-wave excitations. Both Metglas alloys 2605SA1 and 2605S3A have received significant interests in recent years, but 2605SA1 shows comparatively better performance especially in high-frequency applications. Fig. 5 shows the comparison of B-H characteristics of amorphous alloy 2605SA1 and 2605S3A under square-wave excitations.

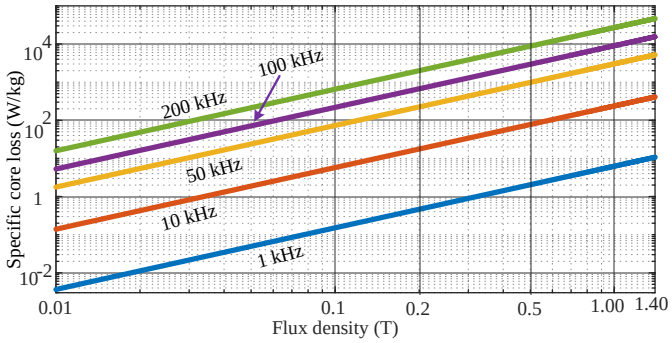

Fig. 4. Core loss of amorphous alloy 2605SA1 under square-wave excitations.

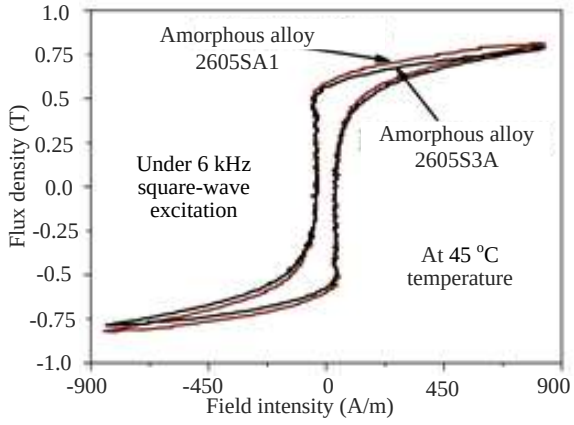

Fig. 5. Comparison of B-H characteristics of amorphous alloy 2605SA1 and 2605S3A under square-wave excitations.

Vendors provide core loss data under sinusoidal excitation which can be used to design the line frequency transformer but not useful in applications as the core loss significantly increases with non-sinusoidal excitation.

V. Simulation Results and Discussion

This section presents the simulation results obtained from the proposed magnetic bus-based NPC converter system using the proposed FCS-MPC scheme. The detailed simulation studies have been conducted using MATLAB/Simulink environment. Fig. 6 shows the converter output voltage v_c and the grid current i_g. Fig. 7 shows the frequency spectrum of the simulated line current of the proposed converter.

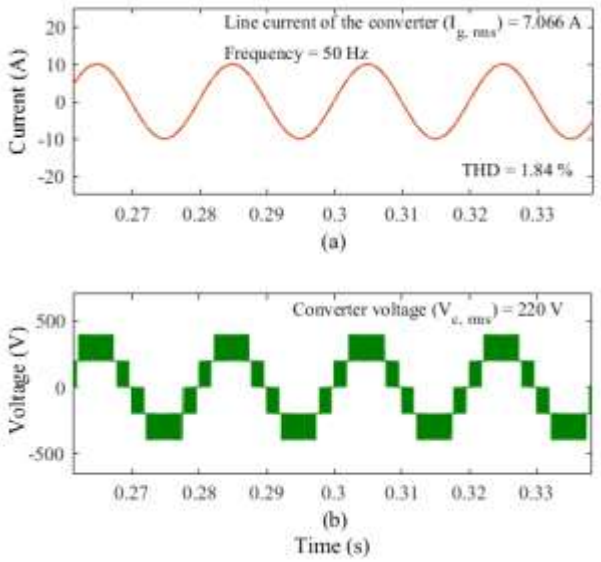

Fig. 6. Simulated output of the proposed magnetic-link based converter: (a) line current, and (b) voltage.

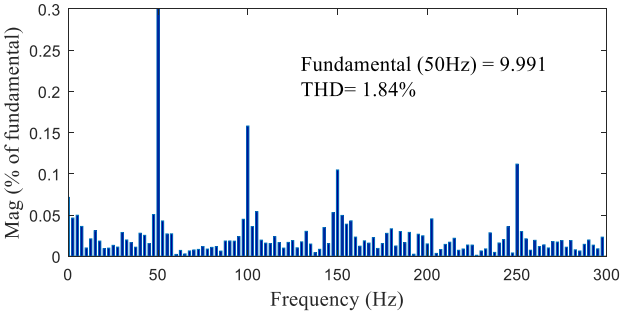

Fig. 7. Frequency spectrum of the simulated line current of the proposed converter.

As it can be seen that five distinct voltage levels i.e., $+V_{DC}$, $+V_{DC}/2$, 0, $-V_{DC}/2$, $-V_{DC}$ are generated at the output of the inverter. Fig. 8 shows the voltage waveforms across the series capacitors of the proposed magnetic bus-based converter without using any additional controller to balance capacitor voltages. It can be seen clearly that each capacitor voltage is maintained at $V_{dc}/2$, and consequently, five distinct voltage levels are observed in the ac-side. The performance of the proposed converter is also compared with that of the traditional NPC converter. Fig. 9 shows the results associated with the conventional NPC converter without using capacitor voltage balancing strategy. As it can be seen that, the output

voltage waveform of the inverter (v_c) and series connected capacitor voltages (V_{C_1}, V_{C_2}) are distorted, and consequently, this increases the THD of the grid current.

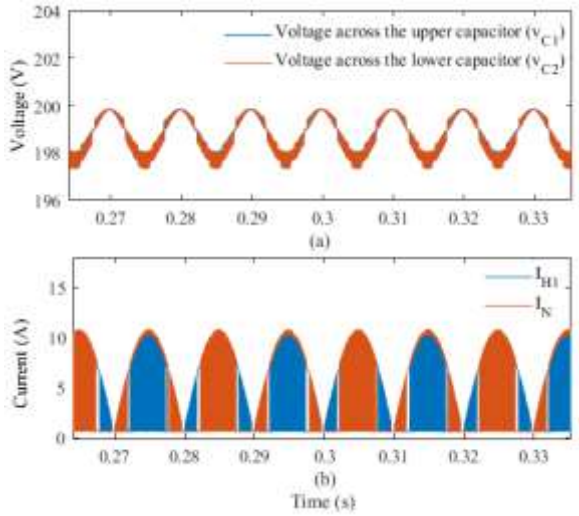

Fig. 8. Simulated output of the proposed magnetic bus-based converter: (a) series connected capacitor voltages (V_{C_1}, V_{C_2}), and (b) internal current waveforms (I_{H1}, I_N).

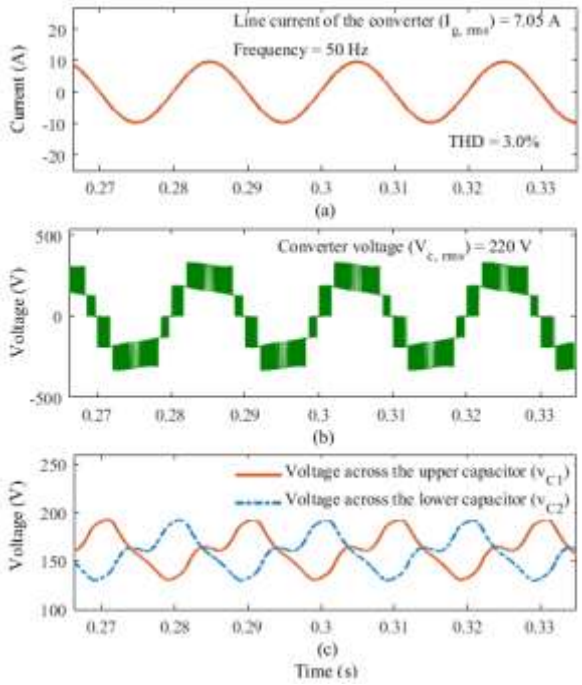

Fig. 9. Simulated output of the conventional NPC converter: (a) line current, (b) output voltage and (c) series connected capacitor voltage waveforms.

To evaluate the performance of dynamic active and reactive power tracking of the derived control system, a step variation in the reference active power reference is introduced from 1000 to 1500 W at 0.3 s, and reactive power reference is introduced from 0 to 600 VAR at 0.35 s. Fig. 10 shows the transient response of the proposed controller for the active and reactive power references step changes. It is clear that, the converter output active and reactive power change instantaneously according to the reference active power and reactive power reference values after transient period.

VI. Experimental Results and Discussion

This section presents the prototype test platform and experimental results of the proposed magnetic bus-based 5L-NPC converter with the proposed FCS-MPC based control scheme. In this paper, a 2.5 kVA high-frequency magnetic bus made with core of amorphous ribbon 2605SA1 and windings of Litz wires (single primary and two secondary) is used to generate isolated and balanced dc supplies for the NPC converter. Approximately 1 kg amorphous ribbons (20 µm thick and 25 mm wide) were used to develop the core with a volume of 135 cm^3. Litz wires were developed with 13 isolated strands (insulated coper wire) of 0.44 mm each. The primary and secondary windings have 20 turns on each with a dc resistance of 0.033 Ω. The magnetic bus inherently ensures the galvanic isolation of the system. Fig. 11 shows a photograph of the high-frequency magnetic bus.

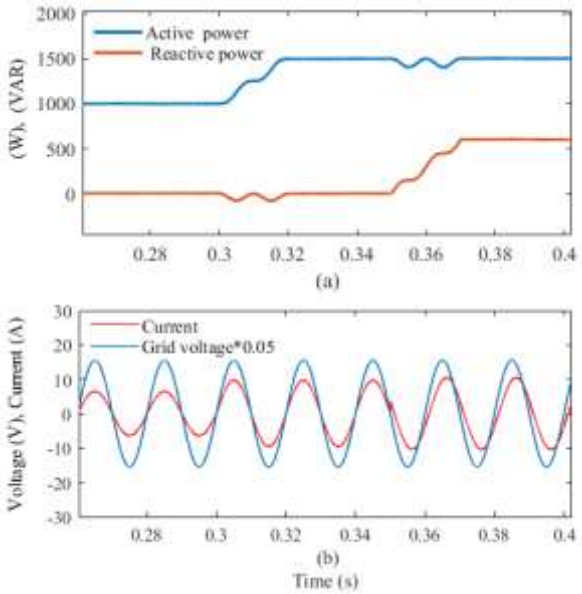

Fig. 10. Simulation results of the proposed converter: (a) active and reactive power step responses, and (b) corresponding injected current and grid voltage waveforms.

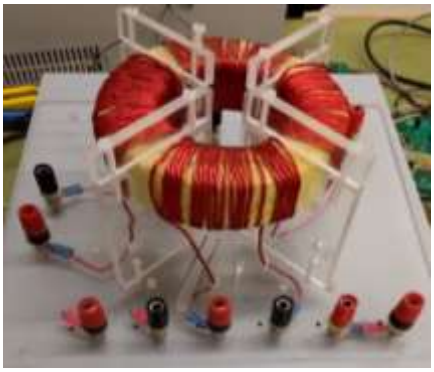

Fig. 11. A photograph of the developed multi-windings magnetic bus with amorphous alloy 2605SA1 based core and Litz wire windings.

The specifications of the test platform are listed in Table II. A photograph of the experimental setup is shown in Fig. 12. ROHM Semiconductor's **N**-channel SiC power MOSFET SCT3022ALGC11 and International Rectifier's ultra-fast

recovery diode HFA15PB60 are used to develop the SiC 5L-NPC converter. The control algorithm is programmed in a digital signal processor TMS320F28379D. The time required by the different control tasks of the proposed algorithm is presented in Table III, which was measured by using the available features in the Code Composer Studio from Texas Instruments. A timer is programmed to acquire the voltage and current sensors data with a sampling frequency of 50 kHz.

TABLE II
SPECIFICATIONS OF THE EXPERIMENTAL SETUP

Parameters	Value	Unit
Sampling frequency	50	kHz
Maximum switching frequency	25	kHz
Filter capacitor	1.0	μF
Filter inductor	5.0	mH
Input ac voltage	150	V
Grid Frequency	50	Hz
Main control chip	TMS320F28379D	
Voltage sensor	LV 25-P/SP5	
Current sensor	LA 25-NP	
Switch (S_1–S_6)	SCT3022ALGC11	
Diode (D_1–D_2)	HFA15PB60	

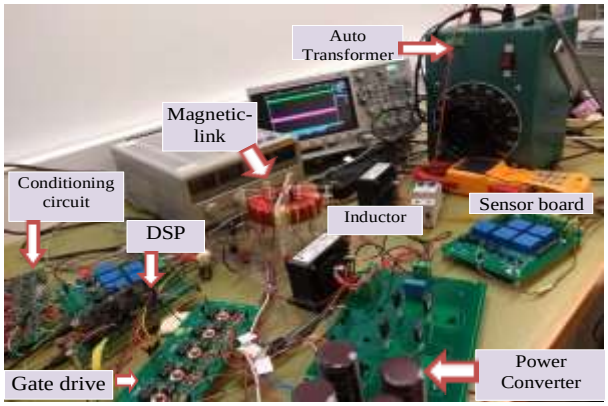

Fig. 12. A photograph of the experimental test platform.

TABLE III
TIME REQUIRED BY DIFFERENT TASKS OF THE CONTROL ALGORITHM

Task	Value	Unit
PLL Synchronization	200	ns
MPC	720	ns
Power controller	200	ns
Current reference generation	29	ns
ADCs reading	32	ns
Gate pulses	165	ns

The Keysight Oscilloscope DSOX2004A with the Tektronix high-voltage differential probe P5200 and current probe TCPA300 are used to measure the voltage and current of the system. The zoomed version output voltage and current of the converter are illustrated in Fig. 13(a). As it can be seen, the maximum switching frequency of the converter is 25 kHz with the derived FCS-MPC control algorithm. The performance of the proposed magnetic bus-based energy conversion system and the associated control technique was evaluated for the adopted 5L-NPC inverter where the required voltage balancing technique was not considered during the derivation of the control algorithm. Fig. 13(b) demonstrates the inverter output voltage and the series connected capacitor voltages with the cost function defined in (28) with the derived FCS-MPC algorithm. Capacitor voltages (V_{C_1}, V_{C_2}) are maintained around at the required voltage levels for the NPC inverter, and consequently, five distinct voltage levels are observed in the ac-side of the inverter.

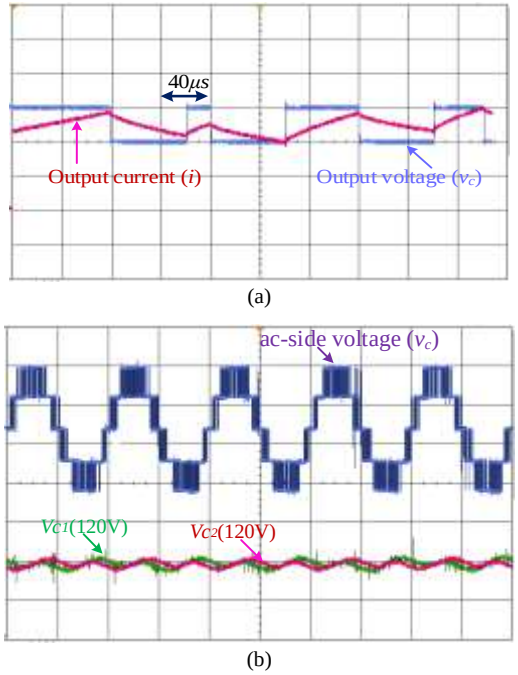

Fig. 13. Experimental performances of the proposed magnetic bus based power conversion system, (v_c: 60 V/div), (v_{c1},: 60V/div), (v_{c2},: 120 V/div): (a) zoomed version output voltage and current of the converter, and (b) converter output voltage and voltage across of capacitors.

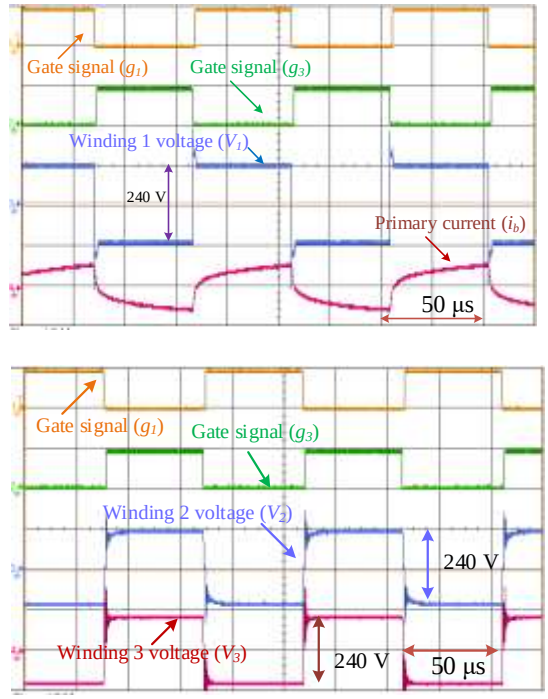

Fig. 14. Experimental performances of the magnetic bus: (a) gate pulses of the high-frequency inverter and excitation voltage and current and (b) induced voltages in the secondary windings.

The high-frequency magnetic bus was excited with a high-frequency inverter circuit. The gate pulses of the inverter circuit and corresponding excitation voltage and current of the magnetic bus were measured, as shown in Fig. 14(a). The induced voltages in the secondary windings of the high-frequency magnetic bus were also measured as shown in Fig. 14(b). To assess the dynamic performance of the proposed system in realizing the reactive power compensation capability, a reference reactive power is introduced in the system. Fig. 15 shows the experimental voltage and line current of the proposed converter after line filter when the employed inverter achieves the expected reactive power reference value.

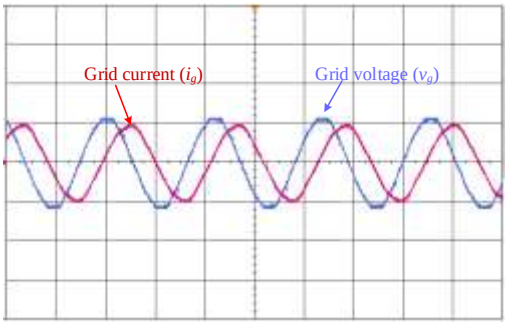

Fig. 15. Experimental voltage and line current of the proposed converter after line filter circuit when employed inverter is achieving the expected reactive power reference value, (v_g: 200 V/div), (i_g: 4 A/div).

VII. Conclusion

Amorphous soft magnetic materials are found suitable for the development of high-power density core of the high-frequency magnetic-bus due to their excellent electromagnetic properties. In this paper, an amorphous alloy magnetic bus is proposed to generate the balanced dc supplies for the 5L-NPC converter for high-quality power conversion. Compared to the traditional converter, the proposed efficient and high-power density magnetic bus-based architecture does not require any control technique for voltage balancing of the series connected capacitors of the NPC converters. Thus, it reduces the control complexity and the size of the boosting inductors. Moreover, the magnetic bus inherently provides the required galvanic isolation for the power conversion systems.

References

[1] Y. Xu, N. Maki, and M. Izumi, "Performance comparison of 10-MW wind turbine generators with HTS, copper, and PM excitation," *IEEE Trans. Appl. Supercond.*, vol. 25, no. 6, p. 5204006, Dec. 2015.

[2] J. X. Jin *et al*., "HTS power devices and systems: principles, characteristics, performance, and efficiency," *IEEE Trans. Appl. Supercond.*, vol. 26, no. 7, p. 3800526, Oct. 2016.

[3] Y. Xu, N. Maki, and M. Izumi, "Overview study on electrical design of large-scale wind turbine HTS generators," *IEEE Trans. Appl. Supercond.*, vol. 28, no. 5, p. 5206905, Aug. 2018.

[4] Z. Deng *et al*., "Pulsed field magnetization properties of bulk Re-Ba-Cu-O as pole-field magnets for HTS rotating machines," *IEEE Trans. Appl. Superconduct.*, vol. 21, no. 3, pp. 1180–1184, Jun. 2011.

[5] J. X. Jin *et al*., "Enabling high-temperature superconducting technologies toward practical applications," *IEEE Trans. Appl. Supercond.*, vol. 24, no. 5, p. 5400712, Oct. 2014.

[6] Z. Deng *et al*., "Trapped flux and levitation properties of multiseeded YBCO bulks for HTS magnetic device applications—part I: grain and current features," *IEEE Trans. Appl. Superconduct.*, vol. 22, no. 2, p. 6800110, Apr. 2012.

[7] J. S. Jeong, D. K. An, J. P. Hong, H. J. Kim, and Y. S. Jo, "Design of a 10-MW-class HTS homopolar generator for wind turbines," *IEEE Trans. Appl. Supercond.*, vol. 27, no. 4, p. 5202804, Jun. 2017.

[8] M. R. Islam, Y. G. Guo, J. G. Zhu, H. Y. Lu, and J. X. Jin, "High-frequency magnetic-link medium-voltage converter for superconducting generator-base high power density wind generation systems," *IEEE Trans. Appl. Supercond.*, vol. 25, no. 5, p. 5202605, Oct. 2014.

[9] M. R. Islam, A. M. M. Rahman, M. M. Islam, Y. G. Guo, and J. G. Zhu, "A modular medium voltage grid connected converter with improved switching techniques for solar photovoltaic systems," *IEEE Trans. Ind. Electron.*, vol. 64, no. 11, pp. 8887–8896, Nov. 2017.

[10] M. R. Islam, Y. G. Guo, and J. G. Zhu, "A multilevel medium-voltage inverter for step-up-transformer-less grid connection of photovoltaic power plants," *IEEE J. Photovolt.*, vol. 4, no. 3, pp. 881–889, May 2014.

[11] R. Sharma, T. W. Rasmussen, and B. B. Jensen, "Application of a synchronous generator with a boost converter in wind turbines: an experimental overview," *IET Renew. Power Gen.*, vol. 6, no. 6, pp. 414–423, Nov. 2012.

[12] A. Kavousi, S. H. Fathi, J. Milimonfared, and M. N. Soltani, "Application of boost converter to increase the speed range of dual-stator winding induction generator in wind power systems," *IEEE Trans. Power Electron.*, vol. 33, no. 11, pp. 9599–9610, Nov. 2018.

[13] S. Iturriaga-Medina *et al*., "A comparative analysis of grid-tied single-phase transformerless five-level NPC-based inverters for photovoltaic applications," *2016 13th Int. Conf. Power Electron. (CIEP)*, 20–23 Jun. 2016, Guanajuato, Mexico, pp. 323–328.

[14] S. Vazquez *et al*., "Model predictive control for single-phase NPC converters based on optimal switching sequences," *IEEE Trans. Ind. Electron.*, vol. 63, no. 12, pp. 7533–7541, Dec. 2016.

[15] S. Wang, W. Song, J. Ma, J. Zhao, and X. Feng, "Study on comprehensive analysis and compensation for the line current distortion in single-phase three-level NPC converters," *IEEE Trans. Ind. Electron.*, vol. 65, no. 3, pp. 2199–2211, Mar. 2018.

[16] A. Sanchez-Ruiz, G. Abad, I. Echeverria, I. Torre, and I. Atutxa, "Continuous phase-shifted selective harmonic elimination and dc-link voltage balance solution for H-bridge multilevel configurations, applied to 5L HNPC," *IEEE Trans. Power Electron.*, vol. 32, no. 4, pp. 2533–2545, Apr. 2017.

[17] V. Yaramasu and B. Wu, "Predictive control of a three-level boost converter and an NPC inverter for high-power PMSG-based medium voltage wind energy conversion systems," *EEE Trans. Power Electron*., vol. 29, no. 10, pp. 5308–5322, Oct. 2014.

[18] V. Yaramasu, B. Wu, S. Alepuz, and S. Kouro, "Predictive control for low-voltage ride-through enhancement of three-level-boost and NPC-converter-based PMSG wind turbine," *IEEE Trans. Ind. Electron.*, vol. 61, no. 12, pp. 6832–6843, Dec. 2014.

[19] V. Monteiro, J. C. Ferreira, A. A. N. Meléndez, and J. L. Afonso, "Model predictive control applied to an improved five-level bidirectional converter," *IEEE Trans. Ind. Electron.*, vol. 63, pp. 5879–5890, Sep. 2016.

[20] J. Ma, W. Song, S. Jiao, J. Zhao, and X. Feng, "Power Calculation for Direct Power Control of Single-Phase Three-Level Rectifiers Without Phase-Locked Loop," *IEEE Trans. on Ind. Electron*., vol. 63, pp. 2871-2882, May 2016.

[21] M. Karimi-Ghartemani, S. A. Khajehoddin, P. K. Jain, A. Bakhshai, and M. Mojiri, "Addressing dc component in PLL and notch filter algorithms," *IEEE Trans. Power Electron*., vol. 27, pp. 78–86, May, 2012.

[22] P. Acuna, R. P. Aguilera, A. M. Y. M. Ghias, M. Rivera, C. R. Baier, and V. G. Agelidis, "Cascade-free model predictive control for single-phase grid-connected power converters," *IEEE Trans. Ind. Electron*., vol. 64, pp. 285-294, Jan. 2017.